

Q-FACTOR ESTIMATION FROM VERTICAL SEISMIC PROFILING (VSP) WITH DEEP LEARNING ALGORITHM, CUDNNLSTM

BEHNIA AZIZZADEH MEHMANDOST OLYA and REZA MOHEBIAN

School of Mining Engineering, College of Engineering, University of Tehran, Tehran, Iran. mohebian@ut.ac.ir

(Received November 16, 2022; revised version accepted January 21, 2023)

ABSTRACT

Azizzadeh Mehmandost Olya, B. and Mohebian, R., 2023. Q-factor estimation from Vertical Seismic Profiling (VSP) with deep learning algorithm, CUDNNLSTM. *Journal of Seismic Exploration*, 32: 89-104.

As seismic reflection waves pass through the different layers and formations of the Earth, they are affected by the attenuation phenomenon that occurs after passing through each layer. One of the most effective and important criteria that can be used in the assessment of attenuation is to check the amount of the Q-value. This value can be used to monitor the amount of attenuation. A key point to remember is that the calculation of Q is always associated with various computational and operational challenges; in other words, the value of Q cannot be calculated in all of the wells that are in a hydrocarbon field.

The purpose of this paper is to present an approach to the problem of estimating the Q-factor by using the latest artificial intelligence method, which is deep learning. By using the CUDNNLSTM algorithm in this paper, we were able to estimate the Q-factor accurately. we achieved an accuracy of 98.5% and a validation loss of 1.3% in estimating the Q-factor. With our Q-factor estimating by deep learning, along with speeding up calculations, we will be able to resolve the problem of lacking suitable VSP seismic data to calculate the Q-factor, as well.

KEY WORDS: Q-factor, Vertical Seismic Profiling (VSP), deep learning algorithm, CUDNNLSTM.

INTRODUCTION

The Quality factor (Q) of seismic waves is a rock property and a measurement of the anelastic attenuation of seismic waves, and it also is a parameter that quantifies the frequency-dependent attenuation through anelastic absorption, which affects the phase and resolution of the seismic signal (Wang et al., 2015; Castagna et al., 2003). In general, high Q-values reveal minimal attenuation, while low Q-values signify significant attenuation (Rubino et al., 2012). Since the downgoing pulse from the VSP can be isolated at each depth down the well, it is like a snapshot of the downgoing wavefield at each geophone depth. Therefore, the VSP provides an ideal opportunity to measure Q directly and observe how its compensation makes an impact on it. The Q-factor is calculated by measuring the changes in frequency content between depth levels (Turhan Taner and Treitel, 2003). In a given frequency band, spectral ratios are calculated between levels, which are determined by the data frequency content. The slope of the spectral ratios can be used as a mathematical equation to determine the value of Q-factor (Matheney and Nowack, 1995). Researchers have presented several different solutions to the issue of determining seismic attenuation in recent decades and many researchers have presented essays on the subject (Xue et al., 2020; Hauge, 1981). Furthermore, it has also been demonstrated that accurate Q-estimation can work to improve the resolution of seismic data, and consequently help better detect hydrocarbons and understand seismic data (An, 2015; Sain and Kumar Singh, 2011). Tonn (1991) showed that when the signal-to-noise ratio is low, the majority of seismic attenuation calculation methods are ineffective, but for high signal-to-noise ratios, the spectral ratio method can be extremely useful (Tonn, 1990). One of the suitable Q-estimation methods is to measure the decrease in wave amplitude with distance. Although this approach, like the rise time approach (Gladwin and Stacey, 1974) and the analytical signal method (Engelhard, 1996), may need to know accurate amplitude data, which is not always available. The attenuation of frequency can also be measured by other methods, such as the spectral ratio method (Hauge, 1981; Blias, 2012; Guerra and Leaney, 2006). Moreover, some researchers have assessed the performance of most of the existing Q-estimation methods, and they found that each of them performed better under different conditions (Tonn, 1990; Jannsen et al., 1985). For a Canadian oilfield, Haase and Stewart applied spectral ratio methods and VSP-sonic drift curves in 2004 to find the Q-factor (Haase and Stewart, 2004). Liu et al. (2018) Proposed a modified log spectral ratio (MLSR) approach that calculates Q-factor from seismic common midpoint (CMP) data. A non-linear inversion of spectral ratios using Levenberg-Marquardt techniques was proposed by Sangwan et al. (2019) as a remedy for the noise sensitivity of conventional spectral ratio methods (Marquardt, 1963; Levenberg, 1944). VSP data was used to verify the accuracy of the estimated Q-factor and it was concluded that the proposed methodology performs

effectively when the signal-to-noise ratio is low (Sangwan et al., 2019). The importance of Q-factor estimation is very wide and in 2021, Vesnaver and his colleagues were able to detection the Geofluid and fractures in the specific geological zone in the Northern Adriatic Sea region using broadband Q-factor (Vesnaver et al., 2021). In 2022, Mirzanejad and et al. using Q-factor for track siemic attenuation and wave propagtion for Full-waveform inversion (FWI) methods by developing 3-dimantional Gauss-Newton optimization (Mirzanejad et al., 2022). In this paper unlike of last research, we foucaed on a new approach to estimate the Q-factor. Deep learning is a subbranch of artificial intelligence that have very complex and robust algorithms for estimating than machine learning algorithms so we developed a new workflow that is based on a deep learning algorithm (CUDNNLSTM) to estimate the Q-factor which has low uncertainty and high accuracy than past estimating Q-factor methods and algorithms.

MATERIALS AND METHODS

Spectral Ratio Q Estimation method

During seismic propagation, we have to characterize the effect of anelastic attenuation on the seismic signal. The anelastic attenuation can be estimated using VSP datasets (Q-factor). Compression waves derived from the VSP are used to characterize the transmission effect of the overburden. To diminish the effects of anelastic attenuation, the Q-factor can be used to derive a Q-filter.

Data from two receiver depths are selected along with an assumed constant Q-medium using spectral ratios as one of the robust and efficient methods for Q-estimation. Accordingly, the spectral amplitude A at frequency and time t_2 is related to the spectral amplitude at time t_1 by:

$$A(f, t_2) = A(f, t_1) e^{-\pi f(t_2 - t_1)/Q} \quad .$$

Rearranging and taking the logarithm,

$$\ln \left[\frac{A(f, t_2)}{A(f, t_1)} \right] = -\pi(t_2 - t_1)/Q \quad .$$

A linear regression of the left-hand side versus frequency therefore yields a slope, which is equal to $-\pi(t_2 - t_1)/Q$. The concept is summarized in Fig. 1. The input variables to Q-estimation using spectral ratio method are the low and high frequency cut-offs optional smoothing parameters.

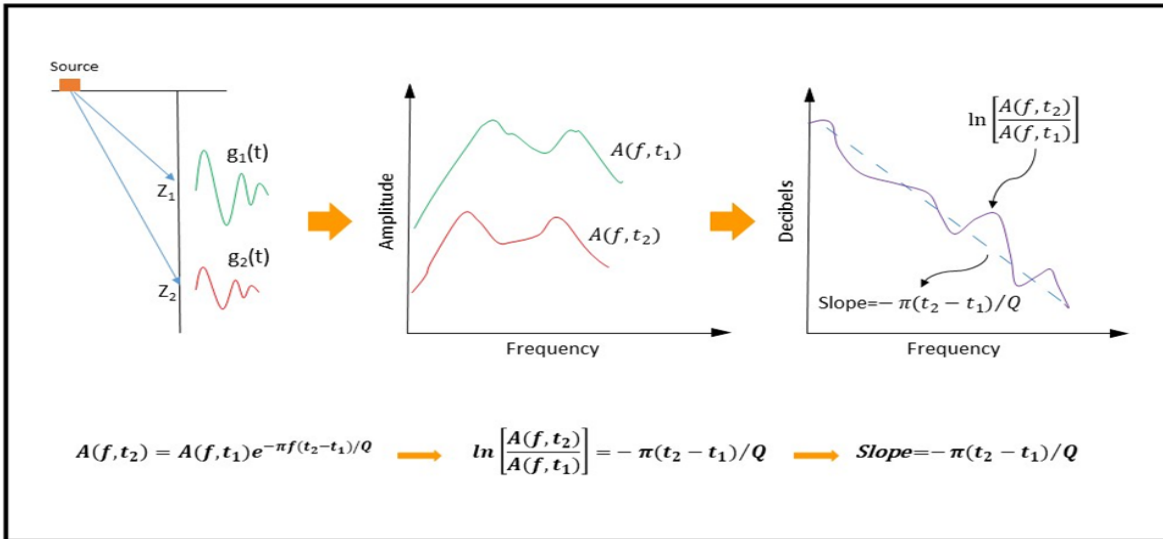


Fig. 1. Principal of spectral ratio Q-estimation method.

General workflow

The general workflow used in this article is shown in Fig. 2. Generally, this workflow consists of two basic parts: training the algorithm and creating the primary data. The above parts will be explained in order.

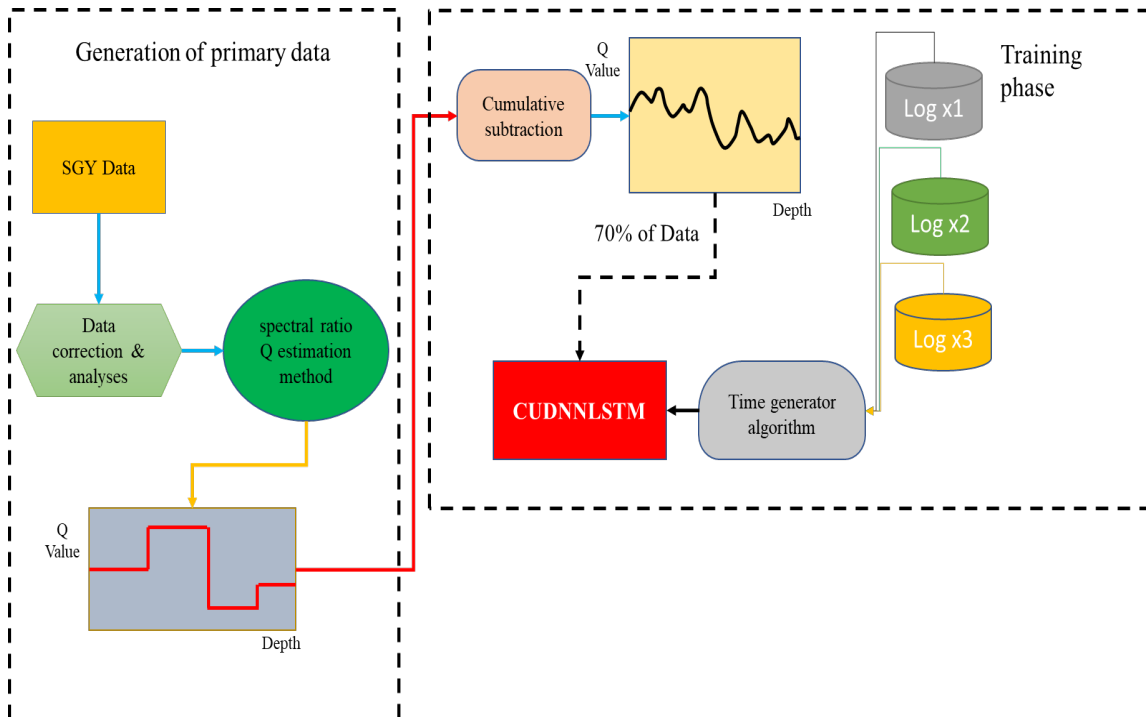


Fig. 2. General workflow.

Primary data Workflow

For the purpose of obtaining the primary data, we first have to correct the data of the SGY file that we have. This includes geometric corrections and corrections of the wave amplitude using the RMS method. This will enable us to obtain the correct primary data.

By separating the upgoing waves from those that are downgoing, we could then use this information to extract a deconvolution filter. As a result of the above process, after performing the Corridorstack process and matching the kinetic seismogram with the well data, we were able to obtain Q-values using the spectral ratio Q-method after performing the process above. As the initial feed of the deep learning algorithm, the Q-value obtained in this part is used (Fig. 3).

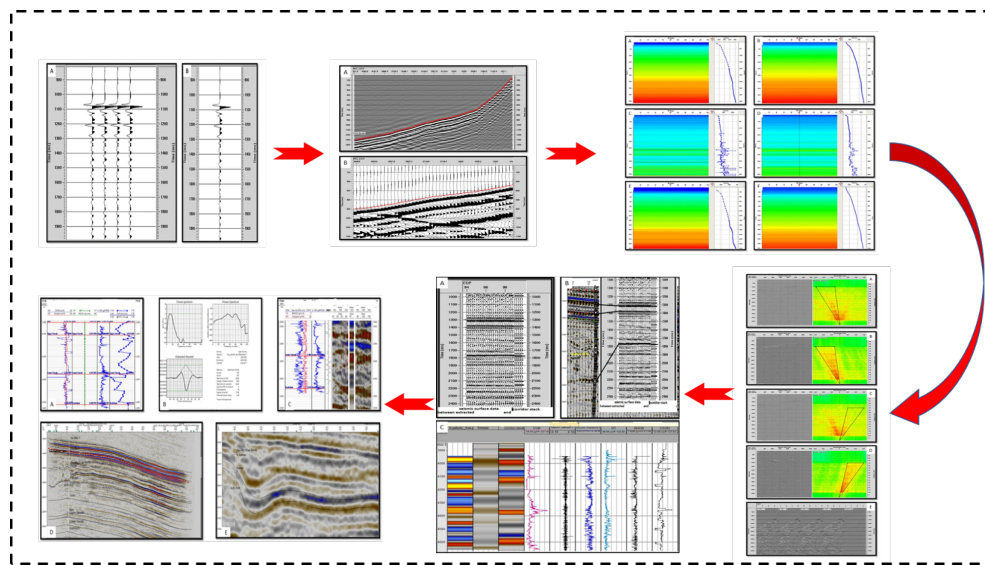


Fig. 3. Primary data process.

PRELIMINARY DATA RESULTS

Calculated initial Q-factor for deep learning algorithm feed

For the purpose of training any deep learning algorithm, as we mentioned at the end of the previous section, we'll need some input data. This section calculates the overall Q-factor for each interval, then converts it to the scale of the logging tool we use by using the cumulative wave amplitude calculation method. The low-frequency and high-frequency cut-offs are input variables to the spectral ratio method for estimating the Q-factor. We need to select a reference level, preferably as high up the well as possible, but we must be careful not to select one influenced by the casing. The spectral ratio method was used to calculate Q for the seismic zones identified in Table 1 and Fig. 4.

Table 1. Seismic horizons and related OWT extracted from VSP data.

| Formation | Measured Depth(m) | One Way Time (OWT) |
|-------------------|-------------------|--------------------|
| Mbr 7 Gachsaran | 1967.5 | 693.76 |
| Mbr 4 Gachsaran | 2225.5 | 768.934 |
| Asmari | 2631.5 | 875.859 |
| Kalhur | 2696.5 | 888.089 |
| Massive Anhydrite | 3021 | 958.618 |
| Pabdeh | 3090.5 | 975.388 |
| Gurpi | 3512 | 1093.45 |
| Ilam | 3905.5 | 1193.98 |
| Upper Sarvak | 4047 | 1220.59 |
| Lower Sarvak | 4386 | 1279.28 |
| TD(VSP) | 4629.6 | 1322.67 |

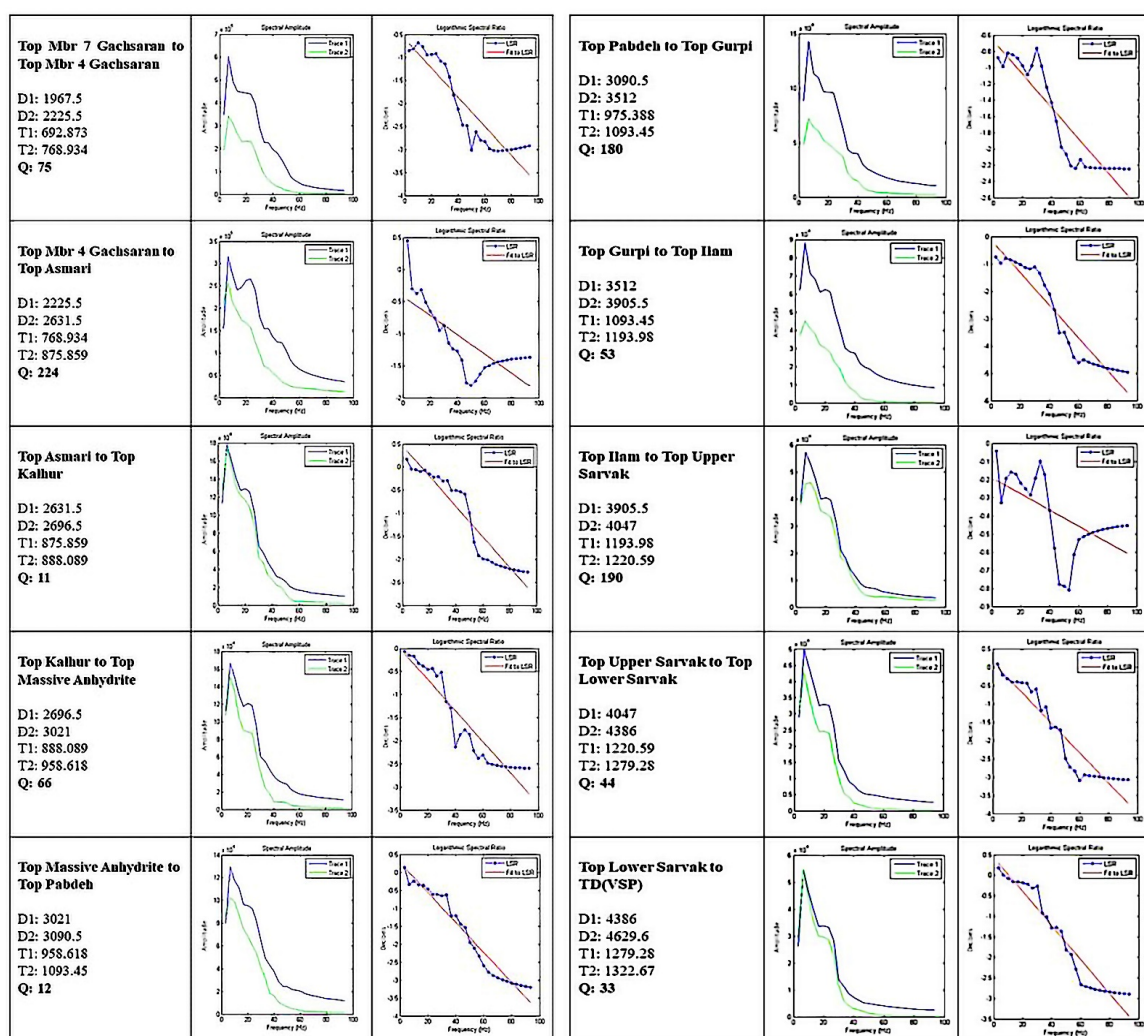


Fig. 4. Q-estimation in different intervals.

Table 2. Formation Intervals and Estimated Q-values.

| Formation Interval | Depth Interval(m) | Q interval | Vint(m/s) |
|---------------------------|-------------------|------------|-----------|
| Mbr_7Gachsaran-Mbr 4 | 1967.5-2225.5 | 75.0 | 3392.014 |
| Mbr 4 Gachsaran-Asmari | 2225.5-2631.5 | 224.0 | 3797.054 |
| Asmari-Kalhur | 2631.5-2696.5 | 11.0 | 5314.8 |
| Kalhur-Massive Anhydrite | 2696.5-3021 | 66.0 | 4600.944 |
| Massive Anhydrite-Pabdeh | 3021-3090.5 | 12.0 | 515.4563 |
| Pabdeh-Gurpi | 3090.5-3512 | 180.0 | 3570.158 |
| Gurpi-Ilam | 3512-3905.5 | 53.0 | 3914.254 |
| Ilam-Upper Sarvak | 3905.5-4047 | 190.0 | 5317.55 |
| Upper Sarvak-Lower Sarvak | 4047-4386 | 44.0 | 5776.112 |
| Lower Sarvak-TD | 4386-4629.6 | 33.0 | 5614.197 |

As can be seen from Table 2, different Q-values were achieved for different formation intervals. Some formations have high Q and the Q-factor is lower for some of them. When the difference between formation lithologies is significant, the seismic wave attenuation is high and vice versa. In addition to formation lithology, pore spaces and filling fluids can affect formation intervals velocity and Q-factor.

Studied intervals include sedimentary deposits from Cenomanian (Sarvak Formation) to Miocene (Gachsaran Formation) and heterogeneity can obviously be observed over the available lithostratigraphic units. Member 7 of the Gachsaran Formation is dominantly comprised of red and gray marl accompanied with high values of Anhydrite. The main difference between member 7 and 4 is the massive Halite (Salt) content. Halite mineral extensively increased over member 4 and it has impacted the physical properties of this member. Due to this salt content the Q-value has been increased. Generally, the Oligo-Miocene Asmari Formation consists of carbonate rocks but in this region, an anhydritic member called Kalhor member together with frequent Halite layers are also available. A massive salt interval is placed at the bottom of Kalhor anhydrites and its thickness reaches to 100 meters. The massive Anhydrite layer placed below the Halite zone is the last anhydritic member observed during drilling and by increasing the depth. this high discrimination between Kalhor to Pabdeh formation in terms of density and velocity produces different Q-values and decrease Q-estimation until 12. The values of marl, clay and carbonate content are increased such that carbonates, clay and gray marls are the predominant components formed Gurpi, Pabdeh, Ilam and Sarvak Formations. Gurpi and Pabdeh Formations are not considered as a reservoir due to lack of effective porosity. Petrophysical properties such as porosity, shale volume, fluid types and saturation are the main components controlling of Q-variation and rock behavior in Ilam and Sarvak Formations. Hereby, variation detected in seismic responses (density, Velocity and Q) along the mentioned units directly related to such petrophysical features.

CUDNNLSTM, Deep learning algorithm

In artificial intelligence today, efficient and diverse algorithms have been developed due to advances in technology and programming, including deep learning algorithms such as CNN and LSTM. A long short-term memory (LSTM) algorithm is based on the basic principles of long and short memory, which were presented by Hochreiter and Schmidhuber (1997). To explain this algorithm very simply and basic, we can say it intelligently selects the data that is needed for the next step and the data that is not needed, based on the effectiveness of each data set. In comparison to the RNN algorithm, the LSTM algorithm has more complex, intelligent structural units, which makes it easier to flow data.

Algorithm architecture and mathematics

An LSTM algorithm consists of a series of sequential processing units placed next to each other. Depending on the input data, each processing unit can make a decision on its own. In Fig. 5, we can see how these units are arranged.

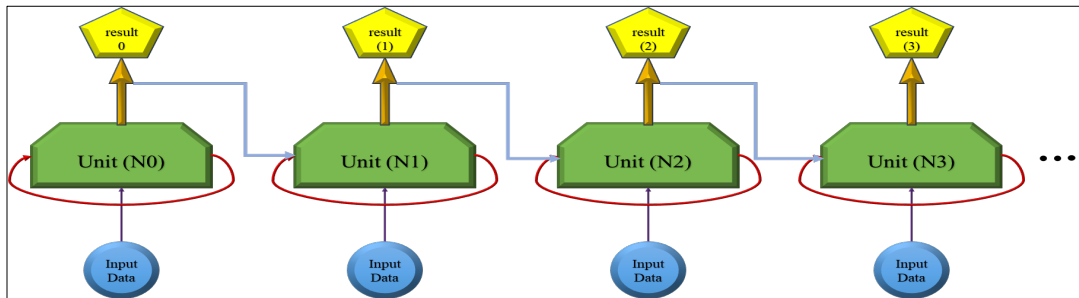


Fig. 5. Algorithm chain overview.

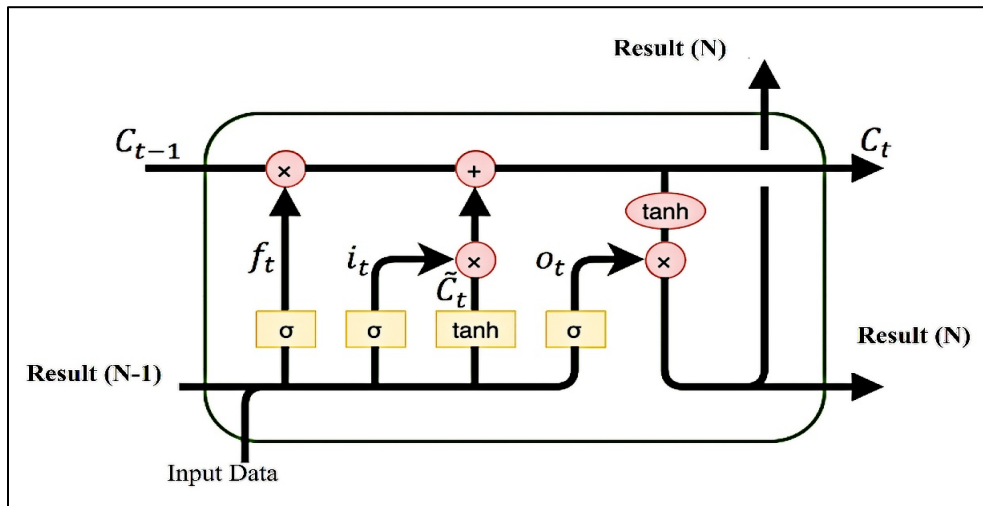


Fig. 6. An overview of each unit's internal structure.

Recursion is one of the reasons for the strength and intelligence of this algorithm, as shown in Fig. 5. This algorithm has a recursive loop, this field allows each unit to act as several separate units. The interior of each unit can be seen in Fig. 6.

According to the LSTM algorithm, data can be intelligently categorized according to its usefulness. Fig. 6 shows that a cell receives 3 inputs, which are input data, result (N-1) and C_{t-1} . Input data represents our data as training, result (N-1) represents the results of the previous unit, and C_{t-1} represents the previous unit's state. It is not always possible to say that an entire data set is useless because it is always possible to extract important information from a data set. To distinguish between valid and invalid data, the LSTM algorithm uses the sigmoid function, which produces a value between 0 and 1. Generally, if the values tend to 0, the data in that cell is not useful, and if they tend to 1, the data is important (Fig. 7).

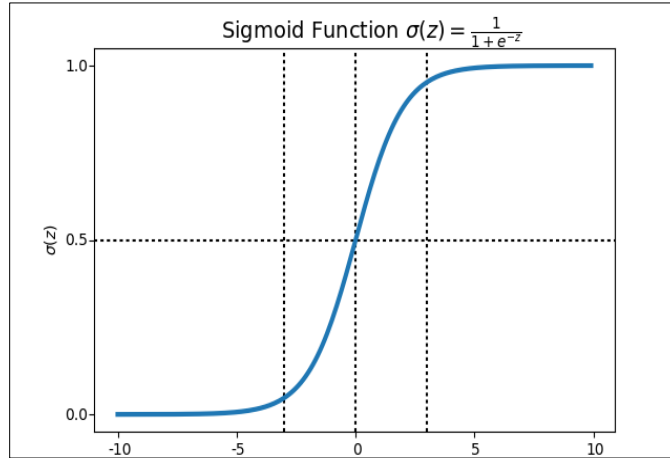


Fig. 7. Sigmoid function.

Input data and result (N-1) paths generally have three sigmoid layers. The first screening is performed between the data's so the first output, which is calculated as follows:

$$f_t = \sigma(W_f \cdot [\text{input data}, \text{result}(N - 1)] + b_f) \quad .$$

After passing through the first gate and multiplying the new data by the state equation of the previous unit, the unit must determine which data needs to be updated. In order to complete this process, the second and third paths are used. Unit data must be updated simultaneously with the equation of state of the cell in order to be updated. A Tanh layer is used to update the new state vectors of the unit, and the second sigmoid layer is used to determine which data needs to be updated. As soon as both of the above are

calculated through the following equations, the values are multiplied by each other, and then the new value is added to the unit state equation.

$$i_t = \sigma(W_i \cdot [input\ data, result(N - 1) + b_i]) \quad ,$$

$$\check{C} = \tanh(W_c \cdot [input\ data, result(N - 1) + b_c]) \quad .$$

Using the sigmoid and tanh functions, we added new equations to the previous unit state equations. According to this equation, the current unit state equation is as follows:

$$C_t = f_t * C_{t-1} + i_t * \check{C}_t \quad .$$

The reason why the equation of state of the previous units flows in the next units is very simple, because the LSTM algorithm is inherently used to recognize series and sequences, so there is always some learning from the previous unit to the new unit to be transferred. The last path involves passing the data through the last sigmoid layer and multiplying it by the state function that passed through the tanh function. As a result of this operation, the unit decides which data to display and which to delete as output. For the purposes of clarity, it is important to point out that all (W) represent the weight and all (b) represent the bias in the equations.

$$O_t = \sigma(W_o \cdot [input\ data, result(N - 1) + b_o])$$

$$result_{(N)} = O_t * \tanh(C_t)$$

The LSTM algorithm, as mentioned, has unique features that make this algorithm a powerful algorithm, but another important point is that, in addition to running on a central processing unit (CPU), this algorithm can be run on a Graphics processing unit (GPU). for this reason, it's great for complex and long sequences because the graphics card has many defense cores called CUDA, which greatly reduces calculation time. The graphite card LSTM algorithm is called CUDNNLSTM.

Designing CUDNNLSTM to estimate Q values

To train supervised algorithms such as CUDNNLSTM, we always need training data and training target data. in this article uses four different logs, RHOB, DT, V_p , and reflection coefficient, because Q-coefficient is directly related to the density and velocity of primary sound waves. Firstly, we screened all the data sets and separated the data that had problems from the main data set so as to make the estimation process more accurate and optimal. Our next step was to design the main network of the algorithm. In the algorithm we used, we put an LSTM with 1500 layers as the main layer and estimator to act as the main processing unit, and then we put a dense neural unit with 300 layers as a correction tool for LSTM output data as well

as an examination tool for LSTM output. All estimator algorithms may suffer from overfitting, so to ensure that throughout the training process there is no overfitting, we used the Dropout operator between the dense layers. Considering that the value of Q-coefficient is always zero or a positive number, we used the relu activation function to prevent negative numbers from entering the training process (Fig. 8).

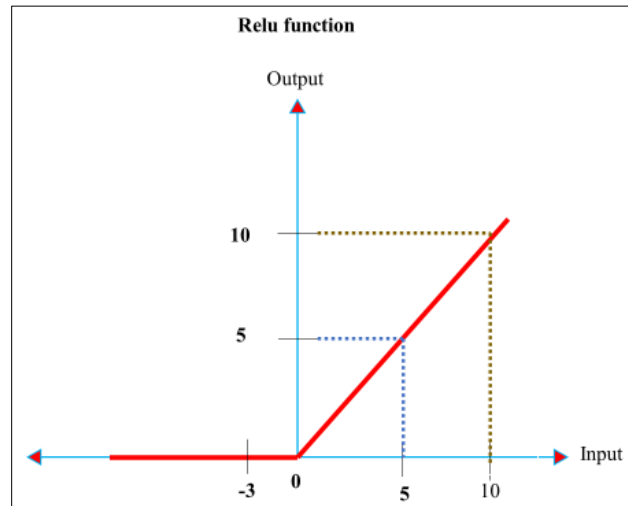


Fig. 8. Relu function.

Our next step is choosing an index to monitor and measure the algorithm's accuracy. The mean square error (MSE) index makes sense based on the nature of the data (series). A point-by-point examination of this index can provide an overview of the difference between result algorithm that estimates and real data. There is no doubt that the higher the MSE index, the better the accuracy of the algorithm and the better the learning process.

It is well known that the log data are point data separated by 0.1524 meters, so in reality, we have a huge set of points separated by a small distance. In the previous section, we mentioned that the CUDNNLSTM algorithm was used to check the series. We used a time generator to convert point data to series data. This generator does not produce time series, but converts our data (logs) into a series structure and then gives the resulting data to the CUDNNLSTM algorithm. Basically, this generator adjusts the scale of the data first and then feeds it in batches to the algorithm. Because of the large volume of calculations, we don't enter the whole series directly into the CUDNNLSTM algorithm, but instead, send it in categories with a series structure (Fig. 9).

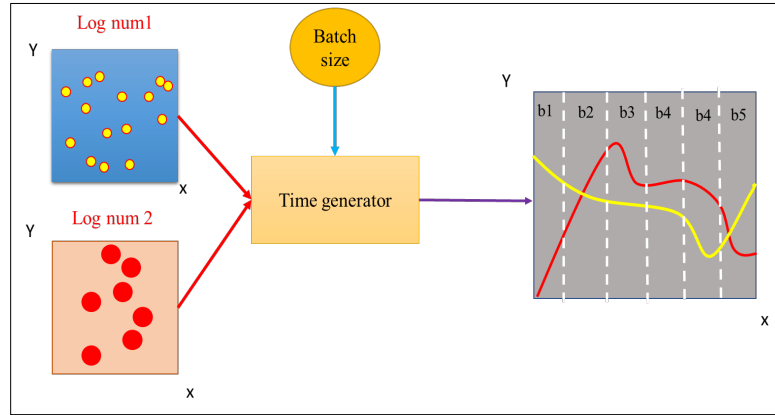


Fig. 9. Time generator.

RESULT

To train the algorithm, we used four different logs (Fig. 10), as mentioned in the previous part:

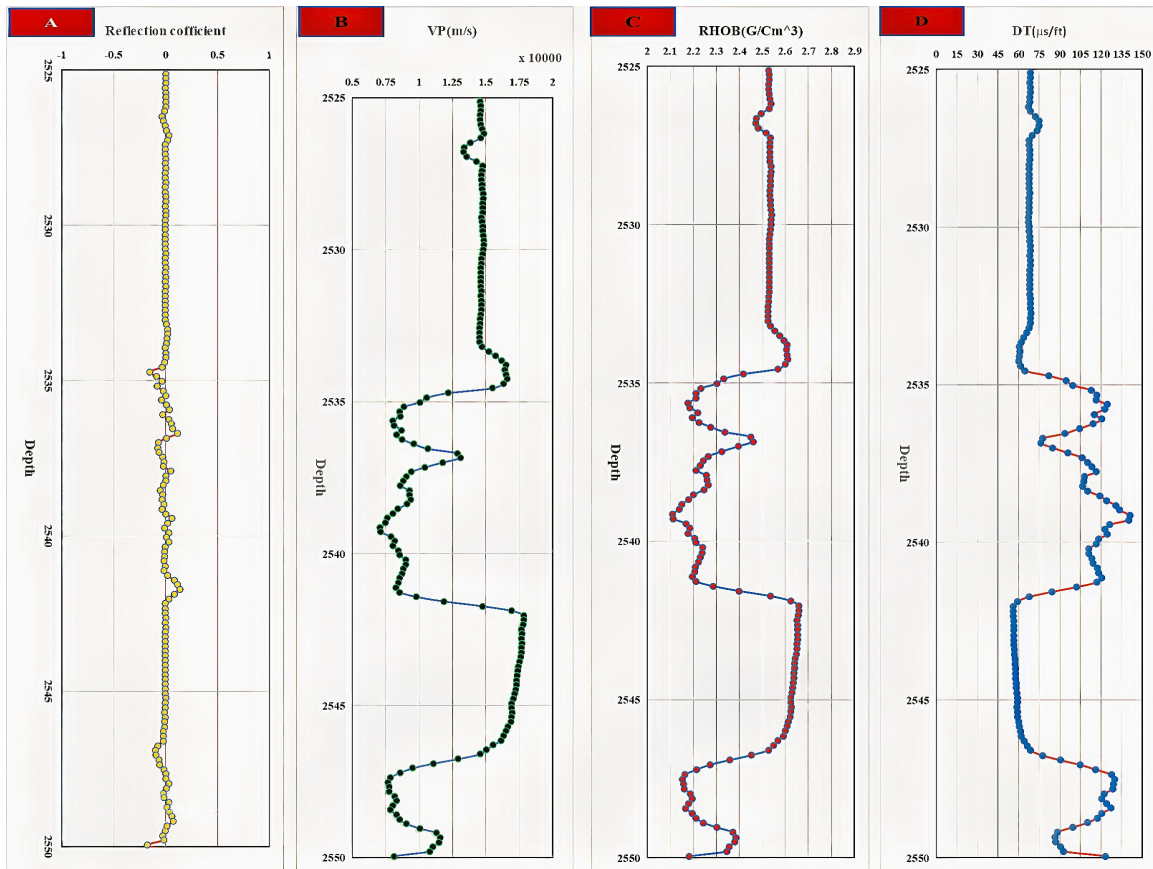


Fig. 10. Logs used: A) reflection coefficient Density. B) primary wave speed. C) RHOB. D) DT.

As it is customary in machine learning, the entire data set is not always used for training; in this case, we had 12694 points, of which we separated 30% of point for testing and validating, or 3809 points. Following the separation of the datasets, the training and target input data are given to the algorithm that was described in the last section. The algorithm was trained for 740 rounds and the accuracy was 98.5% (Fig. 11) and the validation loss was 1.3% (Fig. 12). As mentioned earlier, the above items were calculated using the MSE technique. One of the ways to measure the distance between real data and predicted data by an algorithm is to use the Validation loss (Val_loss) index. In this article, we used it to monitor the changes and improve the performance of the estimator algorithm (CUDNNLSTM).

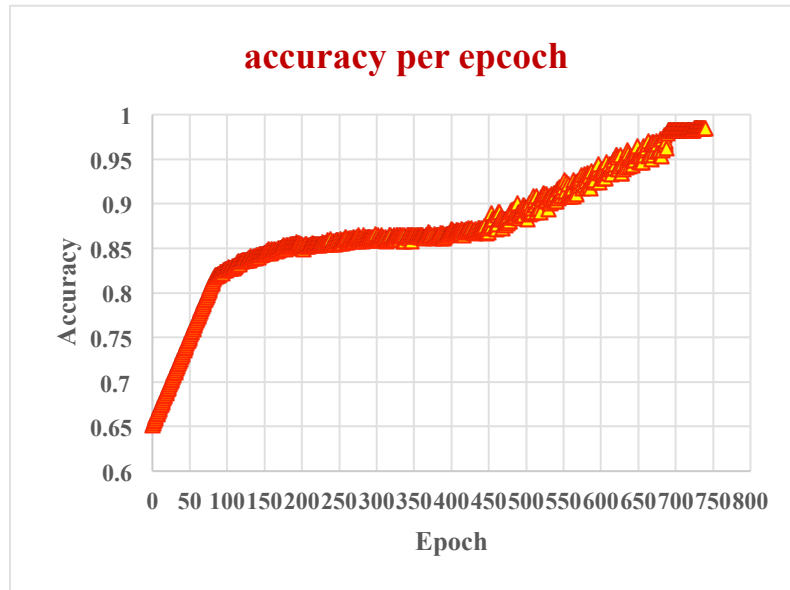


Fig. 11. Accuracy per epoch.

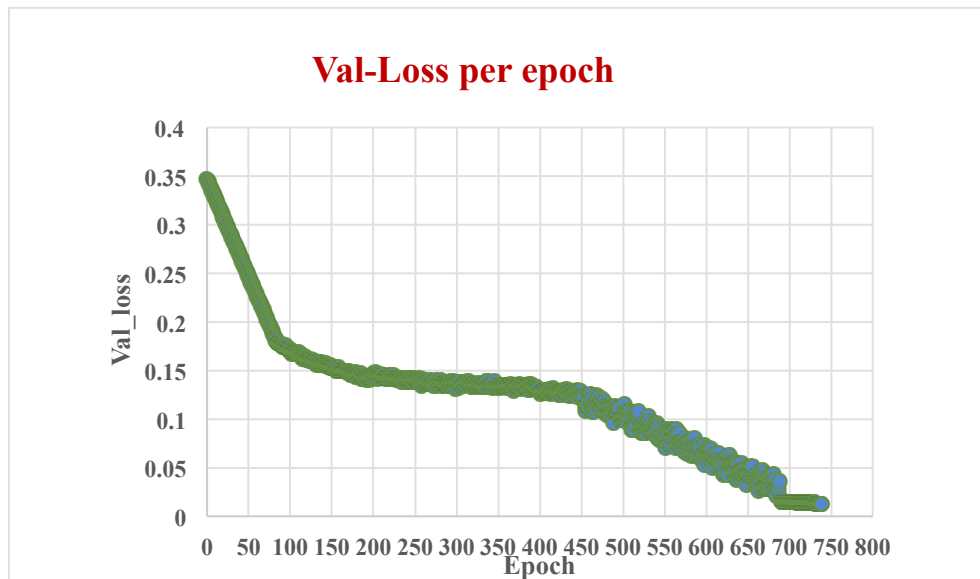


Fig. 12. Validation loss per epoch.

The purpose of this step is to compare the estimated data with the actual data to ensure the algorithm's performance is as accurate as possible (Fig. 13). A key point that needs to be clarified is that, using this trained algorithm, we are able to obtain the Q-value in other wells if there are logs as mentioned earlier. After testing the algorithm, the mean square error (MSE) value obtained was equal to 5.019, which is an excellent number and shows the accurate performance of the algorithm.

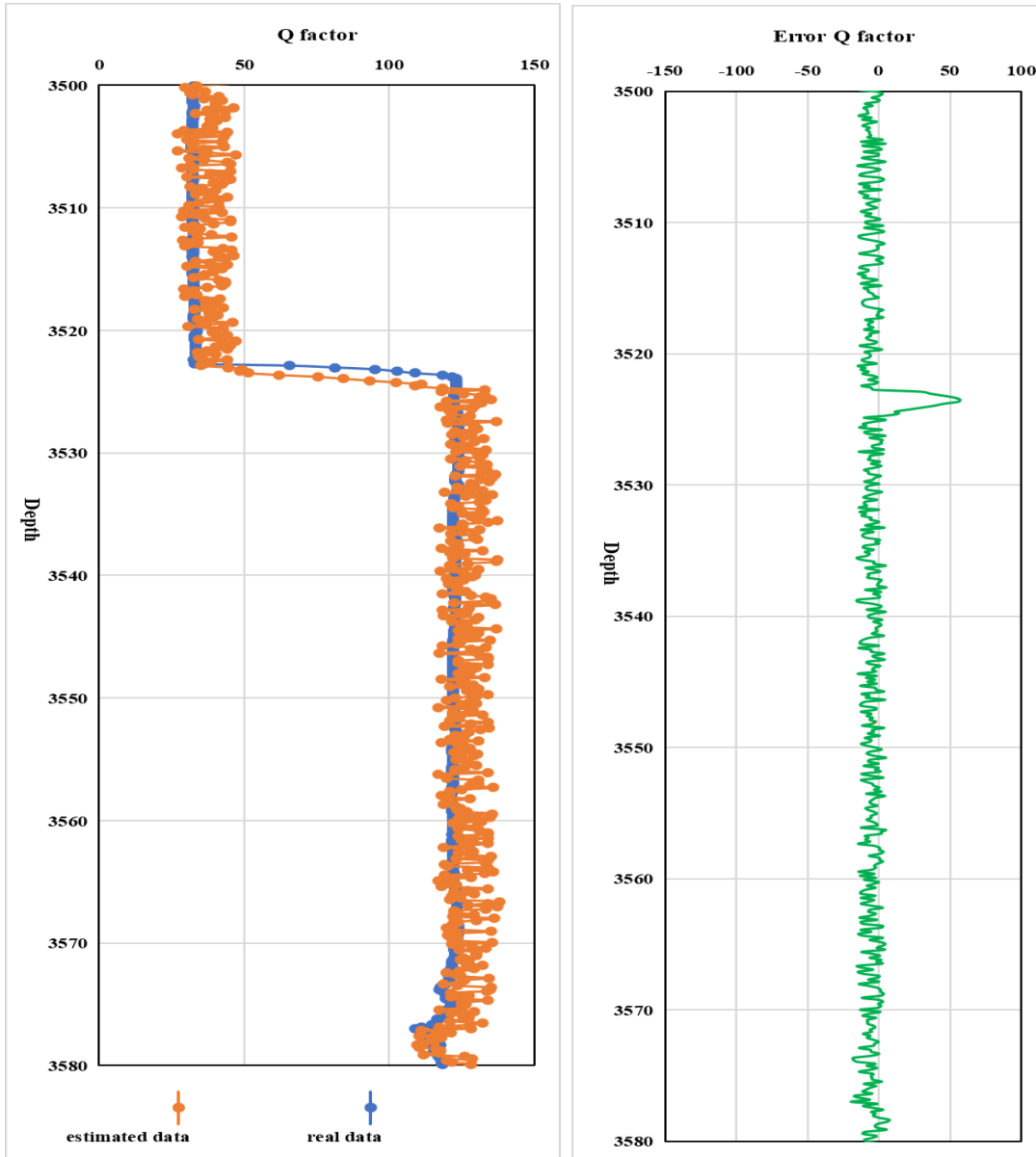


Fig. 13. Data comparison between actual and estimated data and error between real data and estimated data.

CONCLUSION

The results of this research show that the CUDNNLSTM is one of the most robust algorithms for the estimation of the Q-factor in oil fields because the difference between data in unseen well and data estimated by CUDNNLSTM is too low. In addition, because of the logical gate that was mentioned, outlier data can't participate in estimation processes so we had auto-clear data for outliers during of estimating process. The accuracy that we achieved (98.5%) and validation loss (1.3%) shows that this algorithm has a high potential for use in the oil fields that lack VSP data, in other words, we can say the result is a such close to reality and it isn't specific to this data that we use it. The novelties of this research are using a deep learning algorithm instead of the spectral ratio Q-estimation method which has high error and uncertainty, another novelty of this paper is the scale of study. In last methods, Q-factor just estimated in each geological layers, this issue had a lots of side effect such as too much uncertainty because, the geological layers have heterogeneity and there are not pure but, in this essay, we estimated the Q-factor in scale of well logging tools (0.1524 m) so we can track any anomaly that effective on value of seismic attenuation.

In conclusion, we change the estimating approach to use a deep learning algorithm in this article led us to create a new perspective on the Q-factor estimation process, which has several advantages, including accuracy and calculation time.

REFERENCES

- An, Y., 2015. Fracture prediction using prestack Q calculation and attenuation anisotropy. *Appl. Geophys.*, 12: 432-440.
doi:<https://doi.org/10.1007/s11770-015-0493-1>
- Blias, E., 2012. Accurate interval Q-factor estimation from VSP data. *Geophysics*, 77(3): 1M1-J74. doi:<https://doi.org/10.1190/geo2011-0270.1>
- Castagna, J., Sun, S. and Siegfried, R., 2003. Instantaneous spectral analysis: Detection of low-frequency shadows associated with hydrocarbons. *The Leading Edge*, 22: 96-173. doi:<https://doi.org/10.1190/1.1559038>
- Engelhard, L., 1996. Determination of seismic-wave attenuation by complex trace analysis. *Geophys. J. Internat.*, 125: 608-622.
doi:<https://doi.org/10.1111/j.1365-246X.1996.tb00023.x>
- Gladwin, M. and Stacey, F., 1974. Anelastic degradation of acoustic pulses in rock. *Phys. Earth Planet. Inter.*, 8: 332-336.
doi:[https://doi.org/10.1016/0031-9201\(74\)90041-7](https://doi.org/10.1016/0031-9201(74)90041-7)
- Guerra, R. and Leaney, S., 2006. Q(z) model building using walkaway VSP data. *Geophysics*, 71(5). doi:<https://doi.org/10.1190/1.2329866>
- Haase, A. and Stewart, R.R., 2004. Attenuation estimates from VSP and log data. *Expanded Abstr.*, 73rd Ann. Internat. SEG Mtg., Dallas: 2586.
- Hauge, P., 1981. Measurements of attenuation from vertical seismic profiles. *Geophysics*, 46: 1508-1618. doi:<https://doi.org/10.1190/1.1441161>
- Hochreiter, S. and Schmidhuber, J., 1997. Long Short-Term Memory. *Neural Computat.*, 9:1735-1780. doi:10.1162/neco.1997.9.8.1735

- Jannsen, D., Voss, J. and Theilen, F., 1985. Comparison of methods to determine Q in shallow marine sediments from vertical reflection seismograms. *Geophys. Prosp.*, doi:<https://doi.org/10.1111/j.1365-2478.1985.tb00762.x>
- Levenberg, K., 1944. A method for the solution of certain non-linear problems in least squares. *Quart. Appl. Mathemat.*, 2: 164-168.
- Liu, N., Zhang, B., Gao, J., Gao, Z. and Li, S., 2018. Seismic attenuation estimation using the modified log spectral ratio method. *J. Appl. Geophys.*, 159: 386-394. doi:<https://doi.org/10.1016/j.jappgeo.2018.09.014>
- Marquardt, D., 1963. An algorithm for least-squares estimation of nonlinear parameters. *J. Soc. Industr. Appl. Mathemat.*, 11: 431-441.
- Matheney, M. and Nowack, R., 1995. Seismic attenuation values obtained from instantaneous-frequency matching and spectral ratios. *Geophys. J. Internat.*, 123: 1-15. doi:<https://doi.org/10.1111/j.1365-246X.1995.tb06658.x>
- Mirzanejad, M.T., Tran, K. and Wang, Y., 2022. Three-dimensional Gauss–Newton constant-Q viscoelastic full-waveform inversion of near-surface seismic wavefields. *Geophys. J. Internat.*, 231:1767-1785. doi:<https://doi.org/10.1093/gji/ggac287>
- Rubino, J., Velis, D. and Holliger, K., 2012. Permeability effects on the seismic response of gas reservoirs. *Geophys. J. Internat.*, 189: 448-468. doi:<https://doi.org/10.1111/j.1365-246X.2011.05322.x>
- Sain, K. and Kumar Singh, A., 2011. Seismic quality factors across a bottom simulating reflector in the Makran Accretionary Prism, Arabian Sea. *Mar. Petrol. Geol.*, 28: 1838-1843. doi:<https://doi.org/10.1016/j.marpetgeo.2011.03.013>
- Sangwan, P., Kumar, D., Chakraborty, S., Mundayat, V. and Balasubramaniam, M., 2019. Nonlinear approach to spectral ratio method for estimation of seismic quality factor from VSP data. *J. Appl. Geophys.*, 167: 33-41. doi:<https://doi.org/10.1016/j.jappgeo.2019.04.001>
- Tonn, R., 1990. The determination of the seismic quality factor Q from VSP data: a comparison of different computational methods. *Geophys. Prosp.*, 39: 1-27. doi:<https://doi.org/10.1111/j.1365-2478.1991.tb00298.x>
- Turhan Taner, M. and Treitel, S., 2003.. A robust method for Q estimation. Expanded Abstr., 73rd Ann. Internat. SEG Mtg., Dallas: 2452. doi:<https://doi.org/10.1190/1.1818032>
- Vesnaver, A., Böhm, G., Busetti, M., Dal Cin, M. and Zgur, F., 2021. Broadband Q-factor Imaging for Geofluid Detection in the Gulf of Trieste (Northern Adriatic Sea). *Solid Earth Geophys.*, 9: 640194. doi:<https://doi.org/10.3389/feart.2021.640194>
- Wang, S., Yang, D., Li, J. and Song, H., 2015. Q-factor estimation based on the method of logarithmic spectral area difference. *Geophysics*, 80: 1942-2156. doi:<https://doi.org/10.1190/geo2014-0257.1>
- Xue, Y.-J., Cao, J.-X., Wang, X.-J. and Du, H.-K., 2020. Estimation of seismic quality factor in the time-frequency domain using variational mode decomposition. *Geophysics*, 85(4): 1JA-Z18. doi:<https://doi.org/10.1190/geo2019-0404.1>